REPORT DOCUMENTATION PAGE		Form Approved OMB NO. 0704-0188

1. REPORT DATE (DD-MM-YYYY) 18-06-2018	2. REPORT TYPE Final Report	3. DATES COVERED (From - To) 3-Aug-2012 - 11-Mar-2018

4. TITLE AND SUBTITLE Final Report: Classification and Recognition Based on Compressive Spectral Imaging	5a. CONTRACT NUMBER W911NF-12-1-0380
	5b. GRANT NUMBER
	5c. PROGRAM ELEMENT NUMBER 611102
6. AUTHORS	5d. PROJECT NUMBER
	5e. TASK NUMBER
	5f. WORK UNIT NUMBER

7. PERFORMING ORGANIZATION NAMES AND ADDRESSES University of Delaware 210 Hullihen Hall Newark, DE 19716 -0099	8. PERFORMING ORGANIZATION REPORT NUMBER

9. SPONSORING/MONITORING AGENCY NAME(S) AND ADDRESS (ES) U.S. Army Research Office P.O. Box 12211 Research Triangle Park, NC 27709-2211	10. SPONSOR/MONITOR'S ACRONYM(S) ARO
	11. SPONSOR/MONITOR'S REPORT NUMBER(S) 62157-CS.4

12. DISTRIBUTION AVAILIBILITY STATEMENT

Approved for public release; distribution is unlimited.

13. SUPPLEMENTARY NOTES
The views, opinions and/or findings contained in this report are those of the author(s) and should not contrued as an official Department of the Army position, policy or decision, unless so designated by other documentation.

14. ABSTRACT

15. SUBJECT TERMS

16. SECURITY CLASSIFICATION OF:			17. LIMITATION OF ABSTRACT	15. NUMBER OF PAGES	19a. NAME OF RESPONSIBLE PERSON Gonzalo Arce
a. REPORT UU	b. ABSTRACT UU	c. THIS PAGE UU	UU		19b. TELEPHONE NUMBER 302-831-1493

Agency Code:

Proposal Number: 62157CS   **Agreement Number: W911NF-12-1-0380**
INVESTIGATOR(S):

  Name: Gonzalo R Arce
  Email: arce@ee.udel.edu
  Phone Number: 3028311493
  Principal: Y

Organization: **University of Delaware**
Address: 210 Hullihen Hall, Newark, DE 197160099
Country: USA
DUNS Number: 059007500   EIN: 516000297
Report Date: 11-Jun-2018   Date Received: 18-Jun-2018
Final Report for Period Beginning 03-Aug-2012 and Ending 11-Mar-2018
Title: Classification and Recognition Based on Compressive Spectral Imaging
Begin Performance Period: 03-Aug-2012   **End Performance Period:** 11-Mar-2018
Report Term: 0-Other
Submitted By: Joseph Pfister   Email: jpfister@udel.edu
                                               Phone: (302) 831-3142
Distribution Statement: 1-Approved for public release; distribution is unlimited.

STEM Degrees: 3   **STEM Participants:** 4

Major Goals: Please see uploaded PDF

Accomplishments: Please see uploaded PDF

Training Opportunities: During the course of this research program, there were significant opportunities for training. By planning and conducting experiments, graduate and undergraduate students learned methods for electrical and optical measurements, and how to record and analyze complex data. Through productive interactions between University and Army personnel, many technical meetings were held, and Army scientists had opportunities for teaching a University of Delaware course on advanced topics in micro electromechanical systems (MEMS).

Results Dissemination: Please see uploaded PDF

Honors and Awards: Nothing to Report

Protocol Activity Status:

Technology Transfer: Nothing to Report

 PARTICIPANTS:

 Participant Type: PD/PI
 Participant: James Kolodzey
 Person Months Worked: 1.00   **Funding Support:**
 Project Contribution:
 International Collaboration:
 International Travel:
 National Academy Member: N
 Other Collaborators:

 Participant Type: Graduate Student (research assistant)

Participant: John Hart
Person Months Worked: 15.00   **Funding Support:**
Project Contribution:
International Collaboration:
International Travel:
National Academy Member: N
Other Collaborators:

Participant Type: Graduate Student (research assistant)
Participant: Ryan Hickey
Person Months Worked: 9.00   **Funding Support:**
Project Contribution:
International Collaboration:
International Travel:
National Academy Member: N
Other Collaborators:

Participant Type: Graduate Student (research assistant)
Participant: Dominic Imbrenda
Person Months Worked: 14.00   **Funding Support:**
Project Contribution:
International Collaboration:
International Travel:
National Academy Member: N
Other Collaborators:

Participant Type: Undergraduate Student
Participant: David Eldridge
Person Months Worked: 1.00   **Funding Support:**
Project Contribution:
International Collaboration:
International Travel:
National Academy Member: N
Other Collaborators:

James Kolodzey, University of Delaware, June 2018
Final Progress Report for:
Army CERDEC /CPI Project: Advanced Infrared and Terahertz Devices for Navigation, Imaging, Timing, and Ranging

To be submitted On-line at https://extranet.aro.army.mil.
a. A completed "DD Form 882 (Report of Inventions and Subcontracts)
b. "Final Progress Report,"

Final Progress Report for RDRL-ROS-I Proposal Number: 62157-CS; Agreement Number: W911NF-12-1-0380;
Reporting period: 6/1/14 through 3/11/18

Also Submitted to:
Technical Program Manager:
Dr. Gary L. Katulka
Electronics Engineer
Positioning, Navigation, & Timing Branch; Command, Power & Integration Directorate
US Army Communications-Electronics Research Development & Engineering Center (CERDEC)
Building 6007
Aberdeen Proving Ground, MD 21005
<gary.l.katulka.civ@mail.mil>; 443-395-0065

Funding Program Manager:
Dr. Liyi Dai
Department Of The Army
Us Army Research, Development And Engineering Command
Army Research Office
P.O. BOX 12211
Research Triangle Park, NC 27709-2211
< liyi.dai.civ@mail.mil >; (919) 549-4350

Principal Investigator, and University of Delaware Technical Point of Contact:
James Kolodzey
Charles Black Evans Professor of Electrical Engineering
Department of Electrical and Computer Engineering
University of Delaware
140 Evans Hall
Newark, DE 19716-3130; USA
tel: 610-213-3864; fax: 302-831-4316; email: kolodzey@udel.edu;
web: http://www.ee.udel.edu/~kolodzey

Advanced Infrared and Terahertz Devices for Navigation, Imaging, Timing, and Ranging
Final Progress report, June 2018; James Kolodzey, University of Delaware

(1) Foreword

This research program addressed four sub-projects with the goal to develop infrared imaging devices and systems for navigation-based applications to assist US Army personnel. Compared to previous technology, these imaging devices and systems were designed to have smaller size, weight, power, and cost (lower SWAP-C), with improved visibility under dark and obscured viewing conditions such as through smoke and fog. To achieve these goals, our approach included comparing the performance of commercial cameras under different infrared wavelength regions, and evaluating infrared devices made from novel alloys of germanium with tin (GeSn), which have excellent optical properties, and are also compatible with silicon integrated circuit technology for low cost and light weight. The four sub-projects investigated here are: (a) Infrared (IR) detector arrays for computer-based imaging, and software methods to extract the positioning and tracking information; (b) Terahertz frequency devices for covert communication and see-through imaging; (c) Diamond-based resonators for accurate and robust timekeeping; and (d) Energy efficient transistors for ultra-low power circuits. The outcomes of this three-year program included the development and demonstration of prototype imaging methods for compact navigation systems that could operate on battery power. Several new components and methods were developed for evaluation by the Army (Dr. Gary Katulka and colleagues) during periodic visits and technical meetings. The funding level was $100,000 per year to support research personnel, to acquire needed materials and supplies, and for travel to technical meetings and relevant conferences.

(2, 3) Table of Contents and List of Appendixes

Table of Contents

(4) Statement of the problem studied

The challenging problem motivating this research was the development and demonstration of practical imaging systems with low-SWAP-C that could enable navigation in the dark and under obscured visual conditions, but could be carried by Army soldiers in the field. To achieve these goals, this research focused on imaging components and methods, as well as advanced new materials and devices that offered improved infrared performance, but were compatible with silicon integrated circuit fabrication technology, unlike conventional infrared imaging technologies.

(5) Summary of the Most Important Results

During this research program, the following accomplishments were achieved, as described below under the four sub-projects of the original proposal, with their individual sub-tasks.

Project 1: Imaging Arrays with Extended Infrared Operation for Computer Vision-Based Navigation and Tracking

1.1. **Camera Imaging Comparison**. We measured and compared the spectral imaging performance of three commercial infrared (IR) cameras: (A) silicon (Si) CMOS-based Aptina MT9V034 (752H x 480V pixels) in the visible and near IR (400-1050 nm wavelength range); (B) TriWave germanium (Ge) camera (768 x 602 array of Ge photodiodes on Si substrate) with extended response in the near IR (400-1625 nm); and (C) FLIR Merlin/Omega A10 uncooled microbolometer array (160H × 120V pixels) in the far-infrared (7.5-13.5 µm wavelength range). The "subject" for the video cameras was a small toy train enclosed in an airtight 35" x 29" x 15.5" Plexiglas box. Inside the box, different environmental conditions were evaluated: (i) clear air, (ii) smoke from 500 mL of burning pine chips, and (iii) fog from liquid nitrogen added to a beaker of hot water. All three cameras recorded short videos of the moving train, as shown in Fig. 1 below, each with the 3 different levels of obscuring media density: Clear, Intermediate, and Full. Note that "Full" levels of smoke and fog were impenetrable to the two near-IR cameras A and B. Experiments on moving objects under obscured conditions indicated that the FLIR far-IR camera C functioned the best in the *lowest* visibility Full density environments, but was unsatisfactory due to poor visibility under Clear (un-obscured) conditions. As described in Task 1.2 below, the optical transmission through fog and smoke required wavelengths *longer* than about 2.5 µm, with higher transmission at wavelengths longer than 4 µm. Few commercial systems are currently adequate for navigation and see-through imaging under all the obscured conditions investigated here. This finding suggested that a broad spectrum imaging system, such as either a near-IR Si camera combined with a far-IR microbolometer camera, or else a *single* camera with broad spectral response extending from the near-IR (about 1 µm) to the mid-IR (2-5 µm), should ensure continual performance under all obscuring conditions, from Clear to Full obscured, as described in Task 1.3 below.

3

1.2. **Spectral Transmission Through Smoke and Fog**. We evaluated the ability of infrared wavelengths to penetrate environmental smoke and fog. To determine the transmission spectral response, measurements were made with a Fourier transform infrared spectroscopy (FTIR) system (Thermo-Fisher-Nicolet iS50R). A small volume of each environmental medium (smoke/fog) was captured in a transparent plastic bag that was placed between the FTIR light source and detector, and the ratio of intensities between the clear and the obscured paths indicated the net spectral transmittance. Fig. 2 shows the *near*-IR transmission of smoke and fog along with the pass-band wavelengths of three detector materials. Note the trend of increasing transmission with wavelength, and that smoke has less transmission than fog at the longer wavelengths, which is attributed to a combination of its different particle sizes as well as the different chemical compositions. Fig. 3 shows the *far*-IR transmission of smoke and fog along with the pass-band of the FLIR microbolometer camera. Optical transmission through smoke and fog required infrared wavelengths longer than about 2.5 µm, with higher transmission above 5 µm. Based on the imaging results of Task 1.1 above, it was concluded that an optimum photodetector would have a broad spectral response spanning from the near-IR wavelengths (about 1 µm) through the mid-IR (2-5 µm), because this range would enable an imaging system to perform well under all viewing conditions; from clear to fully obscured. Due to the limited wavelength range of conventional photodetectors, however, no commercial imaging system is currently adequate for these imaging applications under the complete range of obscuring environments.

1.3. **Optimal Detector Spectral Response**. Research on infrared transmission and imaging suggested that the optimal IR wavelength range should span from about 1–5 µm for both see-through imaging and navigation positioning with good performance under both clear and obscured conditions. Research suggested that a suitable broad wavelength camera could be developed using photodetector arrays fabricated from alloys of germanium-tin ($Ge_{1-x}Sn_x$) where x is the Sn atomic fraction [1]. Many semiconductor detectors can sense visible and near-IR light (1 µm); the challenge is to extend the long-wavelength limit into the mid-IR and far-IR. As described in Task 1.4 below, with increasing Sn content, the long-wavelength limit of the GeSn detectors increased from the near–IR (1.6 µm) for pure Ge to beyond the mid-IR (>5 µm) for Sn contents greater than about 20% [1-3]. For instance, a camera system using GeSn detectors (with 15.6 % Sn) has response in the 1–4 µm IR range, and could provide adequate performance similar to a Si camera under Clear viewing conditions, as well as adequate visibility in Fully obscured environments. To further extend the upper wavelength limit of the GeSn detectors to above 5 µm, the Sn contents above 15 atomic % were needed, as investigated in this program.

1.4. **GeSn Photodiode Response**. To evaluate the spectral performance of germanium-tin (GeSn) alloys for imaging applications, infrared detectors were fabricated by molecular beam epitaxy (MBE) [2]. The cross section of a typical *p-i-n*-type GeSn photodiode that was fabricated for this project is shown in Fig. 4 (left panel). The MBE growth started on a lightly doped p-type Si wafer substrate, followed by 600 nm of undoped Ge *"virtual substrate"* layer. This was followed by GeSn buffer layers; all wafers had the 9% GeSn buffer (Layer 2), while the higher Sn sample SGS-150 had an additional 15% Sn buffer (Layer 2a) in order to help relieve strain in the upper layers. To evaluate the effects of

composition on spectral response, three photodetectors were fabricated with different Sn contents in the active *p-i-n* detection layers, which totaled about 450 nm thick. Figure 4 (right panel) shows the spectral response of the GeSn *p-i-n* diodes, which detected wavelengths from 1 µm in the near-IR to beyond 2.5 µm, depending on composition. The absolute responsivity of these detectors was uncalibrated, but was normalized for comparison with unity response at photon energy of 0.77 eV (1.61 µm wavelength). For a Sn content of 15.6%, the detector response extended to wavelengths above 4 µm, which showed that GeSn photodiodes are promising for broad wavelength IR applications such as imaging and navigation [1-3].

1.5. **High-Sn Photoconductor Response.** To extend the upper wavelength performance to beyond 4 µm, GeSn detectors with higher Sn contents were fabricated. Using MBE, we grew a series of GeSn alloys with Sn contents up to 31 atomic %, which is one of the highest Sn contents ever reported, on various substrate wafers including silicon (Si), germanium (Ge), and gallium arsenide (GaAs) [2,4]. The goal was to obtain detector arrays for the important mid-IR and far-IR spectral ranges. Due to the difficulty of growing GeSn layers with such high Sn contents, which required growth temperatures below 150 °C, and the difficulty of doping them p-type and n-type, single undoped layers (u-GeSn) were grown on high-resistivity substrates for photoconductivity measurements. To focus attention on the optical properties of the material, and to keep the device structure simple, we investigated a photoconductor design, consisting of a single GeSn layer on a substrate with interdigitated electrodes, as shown in Fig. 5. These GeSn photoconductors had a typical thickness of about 100 nm, with good x-ray diffraction patterns, and the surfaces were specular in appearance, with rms surface roughness about 2 nm, measured by atomic force microscopy (AFM), indicating high quality material. Several GeSn photoconductive detectors were fabricated using Clean Room processing. From the optical measurements shown in Fig. 6, we determined that the photoconductors had a wavelength response spanning from the near infrared to 5 µm for 18% Sn, and up to 7 µm for 21% Sn. As shown in Fig. 7, the broad spectral response demonstrated that GeSn detectors are promising for the required IR imaging and navigation applications.

1.6. **Motion Detection Software**. We evaluated software for analyzing video images, with the goal to determine and interpret the motion of objects under obscured and/or dark conditions. Rather than using a moving camera in a scene of fixed objects, we analyzed a moving subject with a fixed camera, since the principles of motion detection were the same. Videos of moving objects were processed with motion detection algorithms based on MATLAB software that counted the total number of corners of the "subject", which in this case was a small toy (LEGO) electric train, as described in Task 1.1 above. Using MATLAB software, optical flow analysis calculated the direction and rate of the train's movement, recorded the path of travel, and provided output video that displayed vectors along the edges of objects that characterized the motion. Figure 8 shows a screen-capture of a typical output video, with vector arrows indicating the direction of motion. The Open CV software code used for this study is included in Appendix I below. These results showed that software can analyze the video images from IR cameras to extract motion and tracking information that can be used for positioning and navigation. An imaging system that combined a GeSn IR camera with optical flow software should provide a high performance platform for imaging and navigation that can be carried by Army personnel.

1.7.   **Infrared Detector Arrays**. To test the capability of the GeSn photodetectors for video camera applications, *arrays* of detectors were fabricated. To reduce processing complexity, a modest array size of 3x3 pixels was used for the initial prototypes shown in Fig. 9 (left panel). Interdigitated fingers of metals including Al, and multilayers of Ti/Pd/Ag, and Cr/Ag/Au were evaluated as the contact electrodes. Photoconductor arrays were characterized for their spectral response and imaging performance, but the results were inconclusive. The plans were to use IR lenses made from materials including polyethylene, silicon, and germanium, to form images of simple test patterns, such as X's and crosses (+), and to evaluate the array sensitivity and resolution. Depending on the results with small arrays, larger array sizes could be fabricated and tested. To enable the accurate design of optical systems and cameras, the refractive index and optical absorption were measured for GeSn alloys with high Sn contents as shown in Fig. 9 (right panel) [4]. These results showed that GeSn alloys respond to wavelengths beyond 6 µm for Sn contents above 25 %. As mentioned under the previous Task 1.6, GeSn cameras coupled with optical flow tracking software should provide good imaging and navigation capability for U.S. Army personnel, but further testing of detector arrays is needed.

1.8.   **Smart Phone Thermal Camera**. We investigated the miniature commercial *Seek Thermal* cameras (206V x 156H pixels) that attach to "Smart phones" and provide IR imaging in the 7 to 13 µm wavelength band, as shown in Figure 10. Two camera models are compatible with the two common Smart-Phone operating systems (Apple IOS & Android). The first model is the "normal" camera with a viewing angle of 35 degrees and *fixed* focal length for objects located at intermediate distances from the camera. The second model is the "extended range" (XR) camera with a smaller 20 degree viewing angle but *variable* focal length that is more versatile for objects at different distances from the camera. Figure 10 shows a sample view of an IR image on a Smart Phone view screen. This system has not yet been fully characterized by this research program for performance under the imaging environments described in Task 1.1 above, but it seems to be a promising new technology, which could perhaps someday incorporate the novel GeSn detector materials studied here.
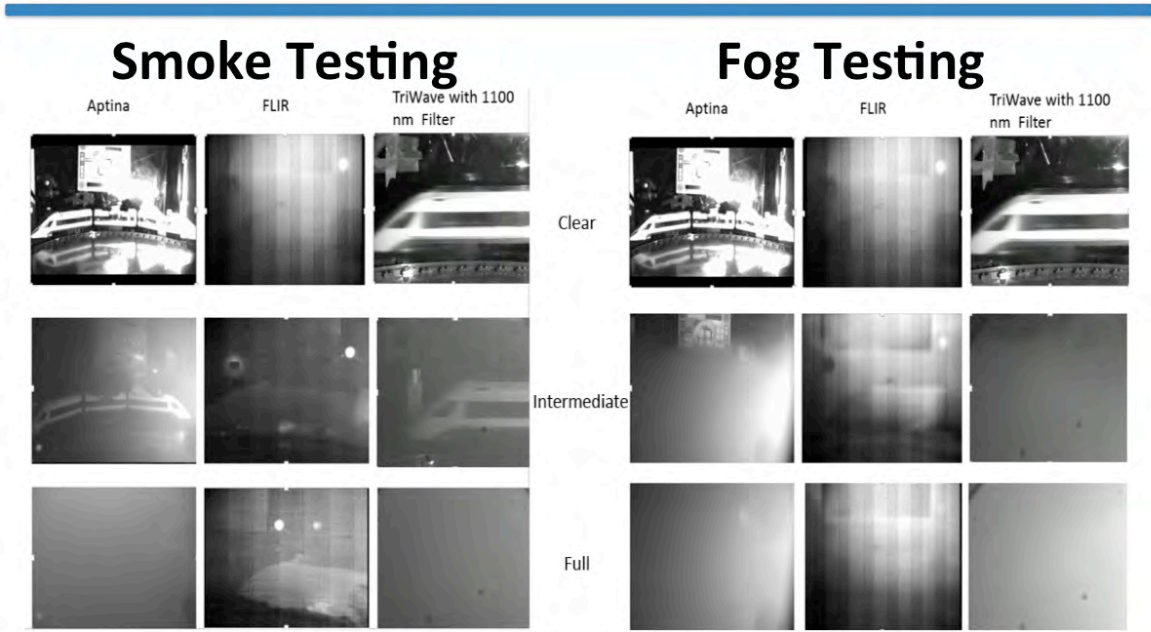
Figure 1. Views of miniature (LEGO) electric train "subject" under three density levels of smoke (left panel) and fog (right panel), for three cameras: Si-based Aptina (near-IR), FLIR microbolometer (far-IR), and Triwave Ge (near/mid-IR) with 1100 nm long-pass filter. Appearance of train is more easily discerned in the upper left and upper right frames of each panel. As media density increased from "Clear" at the top, through "Intermediate" and "Full", the transmission markedly decreased. The far-IR FLIR camera always showed definite transmission in all cases, but was the most difficult to interpret visually under "Clear" conditions.
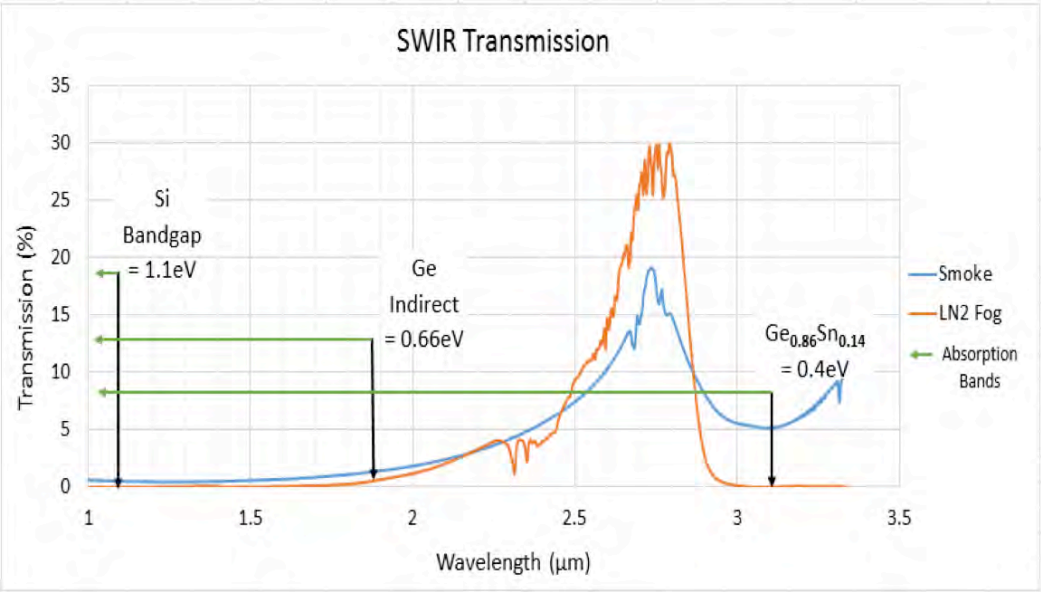
Figure 2. Spectral transmission measurements of fog and smoke in the near-IR, taken with a Fourier transform infrared spectrometer (FTIR) (Thermo-Fisher iS50R). Arrows and rectangles show the pass-band wavelengths of three detector materials; Si, Ge, and GeSn (no camera yet available). The optimum transmission through smoke and fog occurred at wavelengths longer than 2.5 μm.
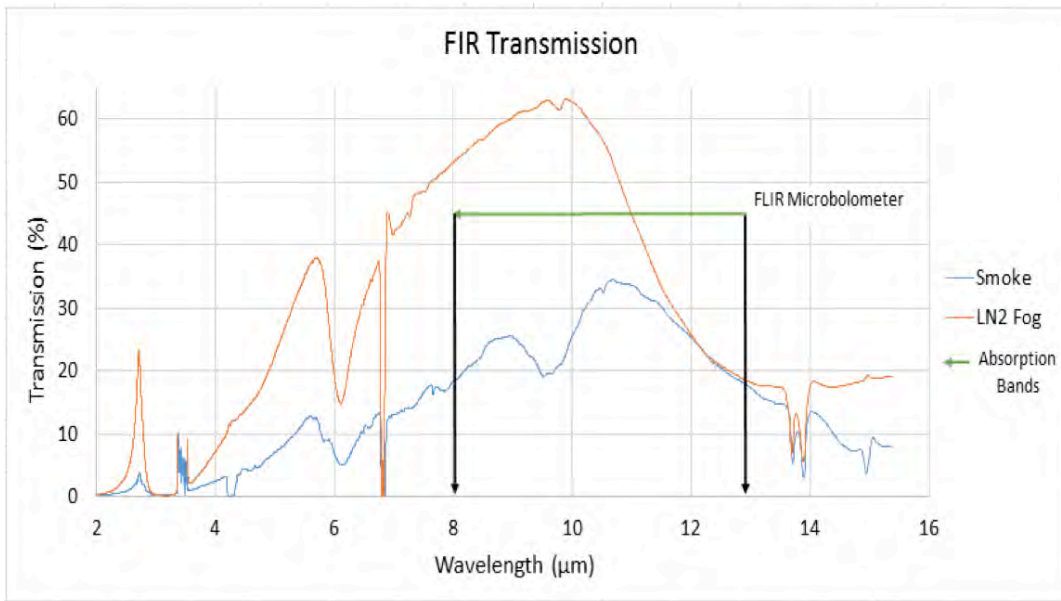
Figure 3. Spectral transmission measurements of smoke and fog in the mid-IR and far-IR, taken with an FTIR spectrometer (Thermo-Fisher iS50R). Transmission through smoke and fog in the mid-IR and far-IR above 4 µm is higher than in the near IR. Arrows show the pass-band of the FLIR Merlin/Omega A10 microbolometer camera.
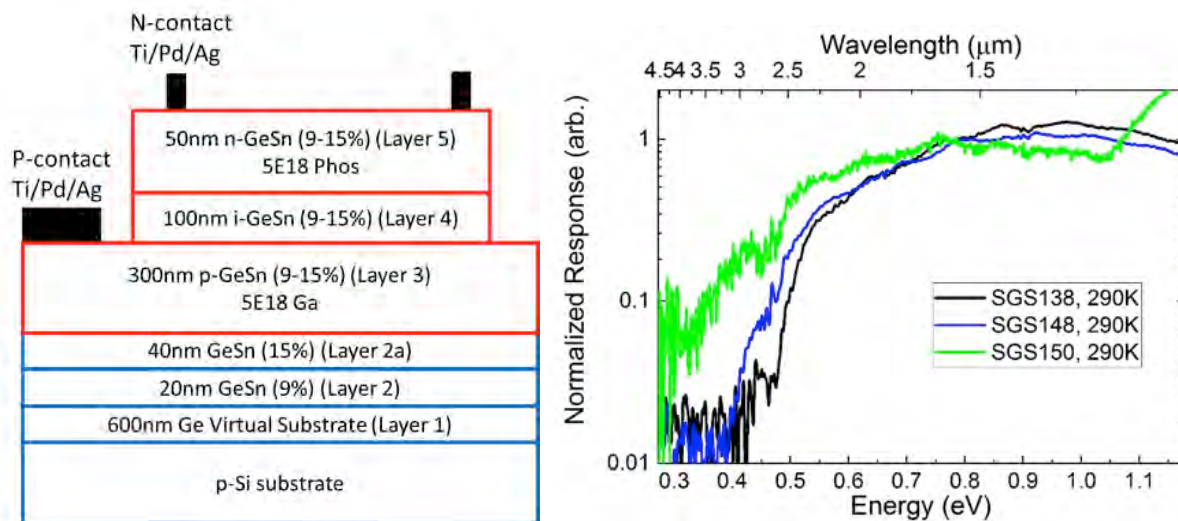
Figure 4. (a. Left Panel) Layer diagram of the GeSn *p-i-n* photodiode that was made with three Sn compositions: SGS-138 (8.9% Sn active layers), SGS-148 (12.8% Sn active layers), and SGS-150 (15.6% Sn active layers). MBE growth was on a p-type Si substrate, and the Ge virtual substrate was undoped. The optically active layers are shown in red, and the blue layers signify non-optically active layers. The Sn concentrations were uniform throughout the active layers. **(b. Right Panel)** Comparison of spectral photoresponse at 290 K temperature of three GeSn diodes with active regions containing up to 15.6% Sn, demonstrating detection from shorter wavelengths to the important wavelengths above 2.5 µm. The data was normalized to the response peak near the photon energy of 0.77 eV (1.61 µm).

8
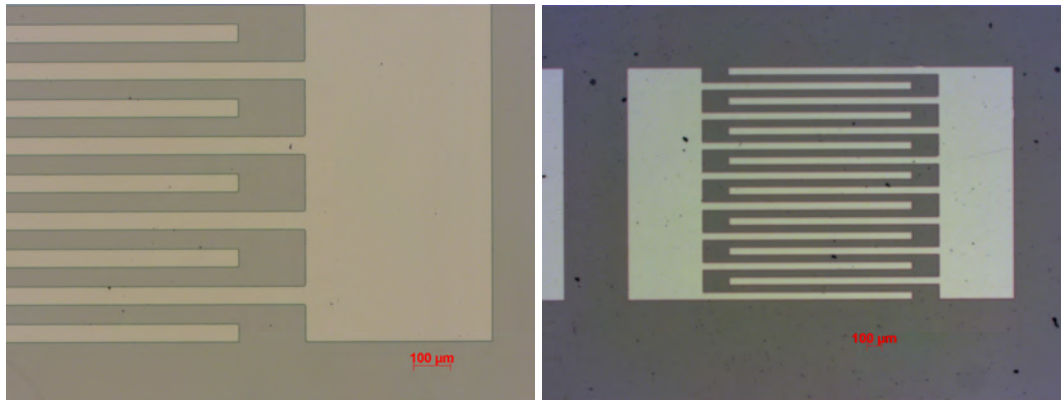
Figure 5. Top view optical micrograph at 5x magnification of GeSn photoconductive detector with interdigitated surface electrodes. Left panel shows the developed negative photoresist after lithographic pattering; bright areas are the GeSn on which metal electrodes (either Al, Ti/Pd/Ag, or Cr/Ag/Au) will be deposited. Right panel shows optical micrograph at 2.5x magnification after Al electrode deposition (500 nm thick). Bright area is the Al and dark area is the GeSn. For reference, 100 μm length scale marks are shown in red font.
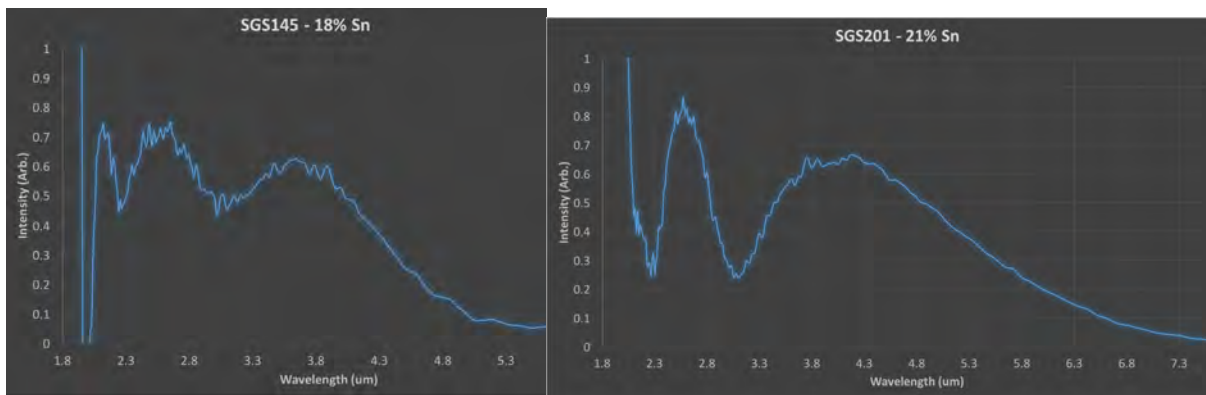
Figure 6. Photoconductive response of GeSn detectors on Ge substrates, illuminated with a broadband IR source (globar) using a KBr beamsplitter. The electrodes were interdigitated finger contacts as shown in Fig. 5, biased at 2V. The left panel shows an 18 % Sn device with response out to a wavelength of about 5 μm, and the right panel shows a 21 % Sn device with response out to about 7 μm. The intensity oscillations at wavelengths from 2–4 μm are attributed to interference effects during the measurements, and are not intrinsic to the GeSn detector.

9
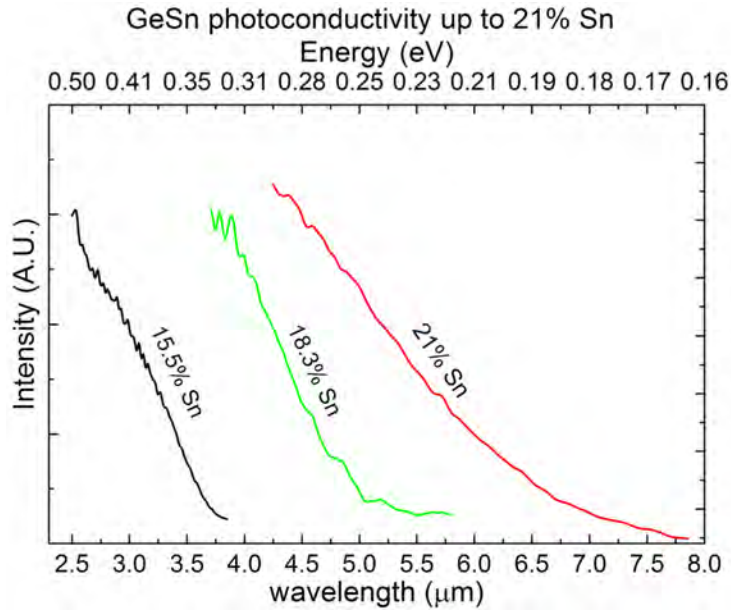
Figure 7. Response of GeSn photoconductor devices with three different Sn contents, on Ge substrates, illuminated with a broadband IR source (globar). The wavelength response increased with the Sn content, and extended to above 7 μm for 21 % Sn. Smaller amounts of Sn can be used at shorter wavelengths, depending on the application [6].
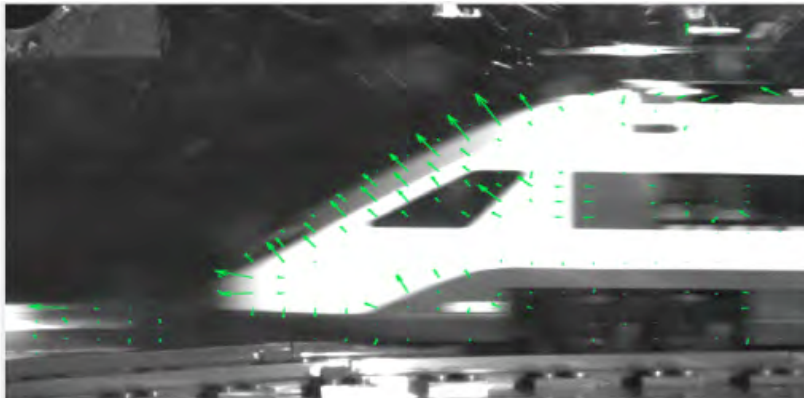
Figure 8. Optical flow analysis of moving LEGO toy train, using Open CV software for motion tracking. The train motion, extracted by the software analysis, is indicated by the green vectors along the edges. The reason for the 45 degree angle (from the horizontal) of the slanted arrows is due to the difficulty of the software to determine if the motion of the slanted edges is vertically upward or horizontally to the left, and so an "average" direction is indicated.
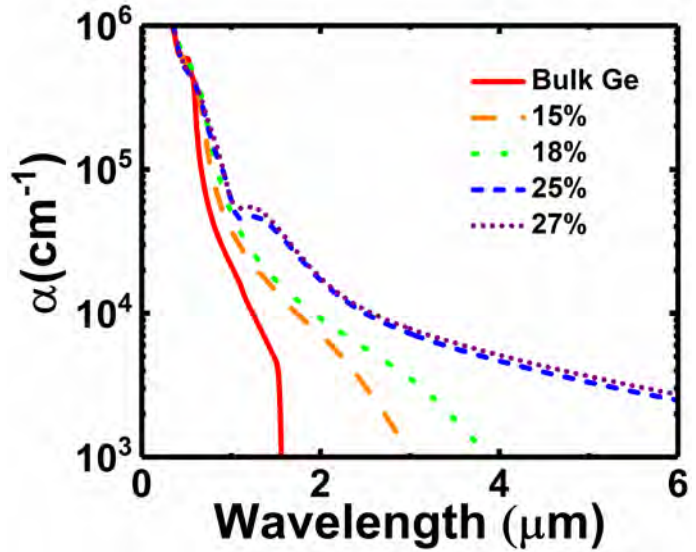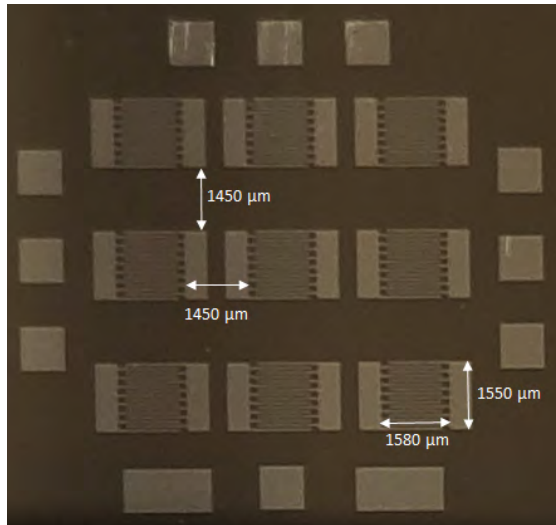
Figure 9. **(a. Left Panel)** Optical image of 3x3 element photodetector array fabricated from a 120 nm thick $Ge_{0.89}Sn_{0.11}$ layer on a Ge substrate. Contact electrodes are 500 nm thick Al metal, patterned via deep UV lithography. Each of the 9 detector elements consists of 8 interdigitated finger pairs that are 1400 µm wide and 50 µm in height. Fingers are spaced by 50 µm. Electrodes connected to each set of fingers are 500 by 1550 µm. Additional electrodes can be made from Au wire-bonds attached to the square pads around the periphery to facilitate measurements. Length scale marks are indicated. **(b. Right Panel).** Absorption coefficient vs. wavelength for $Ge_{1-x}Sn_x$ thin film alloys deposited on Ge wafer substrates. The atomic Sn percentage is indicated by the value in the legend. The minimum plotted value of absorption is 1000 cm^{-1} because ellipsometry measurements are not accurate at lower absorption values. Data for the bulk Ge was taken from published tables [4].

Figure 10. *Seek Thermal* camera attached to the top of an iPhone, showing a typical heat-sensitive image of a running automobile engine.

11

Project 2: Terahertz Emitters and Detectors For Covert Communication and See-Through Imaging

2.1. We evaluated terahertz (THz) emitters that were based on the emission mechanism of intracenter radiative transitions from the dopant atoms in silicon carbide (SiC) p-n junctions [5]. Using calibrated IR detectors that operate in the far-IR and THz ranges (3 THz corresponds to 100 μm) to measure the emitted power, the SiC emitters produced an increasing output intensity versus increasing applied drive current, in the pulsed mode with a 1 % duty cycle. Measurements were repeated at various operating temperatures including room temperature, with greater output intensity at lower cryogenic temperatures, down to 4K. A current versus voltage (I-V) plot of the SiC p-n junction is given in Fig. 11, showing reasonable rectifying behavior, with larger currents at higher device temperatures. Due to a malfunction of the FTIR spectrometer, however, no emission *spectra* of power versus wavelength were yet obtained. The FTIR spectrometer has since been repaired (late 2017), and measurements of the emission spectra are planned.
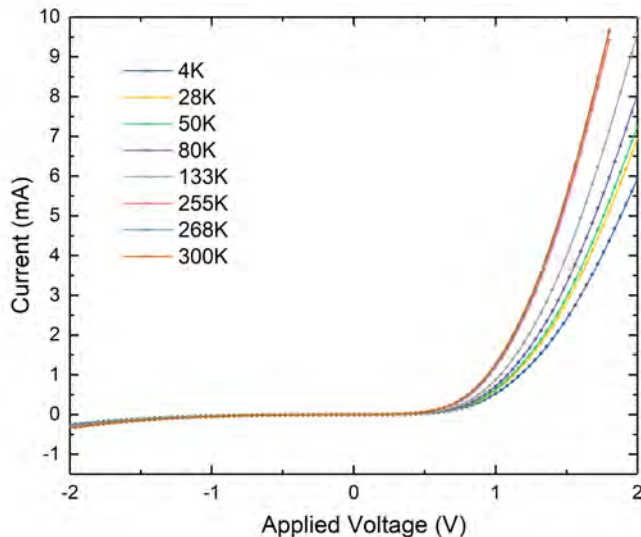
Figure 11. Current versus voltage data for a terahertz emitter based on a SiC p-n junction. As the measurement temperature increased, the current increased for a given applied voltage, which is consistent with the increasing electrical activation of the nitrogen (n-type) and boron (p-type) dopants, as well as to increased carrier diffusion. These SiC devices produced THz emission power (not shown).

Project 3: Diamond Based Mechanical Resonators for High Precision Oscillators and Timekeeping

3.1. No effort on the diamond-based resonator sub-project was performed during this program due to the lack of diamond material.

Project 4: Low Power Transistors and Circuits for Energy Minimization, Long Battery Life, and Low SWAP-C

4.1.   **Low Power GeSn Electrical Devices**. In addition to investigating germanium-tin (GeSn) diodes as infrared detectors, this program also investigated their electrical properties because of the promise for low energy applications. To provide low power circuits for extended operation with long battery life, there are certain fundamental properties of materials and devices that must be considered. These properties include a low bandgap energy (compared to silicon at 1.12 eV), high mobilities of the charge carriers, and low noise operation near room temperature without disruption by the thermal energy $k_B T$ (26 meV at room temperature). To assess their ability to operate at low power levels, devices made from GeSn with low bandgap energy (<0.66 eV) were fabricated, and their electrical characteristics were measured. As described below, the experimental results obtained so far suggest that GeSn devices are promising for Army applications requiring low-voltage, low-power operation.

4.2.   **GeSn Diode Characteristics**. Germanium-tin (GeSn) diodes were fabricated using layers grown by MBE on substrates including Si, Ge and GaAs [2,6]. Standard photolithography was used to pattern the negative photoresist (NR9-3000PY) into meshes for electrical contacts. The top metal electrode was evaporated Ni (30nm)/Al (600nm) on the n-GeSn, and the bottom electrode to the p-Ge was evaporated Al (600nm). Dice containing several diodes were cut using a diamond edged dicing saw. A layer diagram of a typical GeSn/Ge n-p heterojunction diode, and a micrograph of a fabricated device are shown in Fig. 12. Electrical characteristics were measured with a current-voltage (I-V) parameter analyzer. Figure 13 shows typical I-V characteristics, in which the effects of shunt leakage and series resistance were removed using a simple circuit model (also shown in Fig. 13). The diode forward turn-on voltage was relatively low (few tenths of volt), to provide low power operation. The reverse breakdown voltage was also relatively low (a few volts), due to the relatively low bandgap energy (E_g < 0.6 eV). Higher reverse breakdown voltages may be achievable using lower doping concentrations, and/or different device designs such as *p-i-n* structures. During the course of this project, the electrical performance of these GeSn diodes were optimized by evaluating the effects of layer thickness and doping concentration to achieve good rectifying characteristics (high forward-to-reverse current), low turn-on voltage, and relatively high reverse breakdown voltage. Reasonable doping concentrations for GeSn devices seem to be in the mid-10^{17} cm^{-3} range. For reasons that are still unclear, the undoped GeSn had residual p-type conductivity, which is still under investigation.

4.3.   **Weyl Fermions for Dissipationless Electronics**. For the ultimate in low power circuit possibilities, in 2015 a discovery was made of Weyl fermion quasiparticles in the semimetal tantalum arsenide (TaAs), which may support *dissipationless* currents [7]. Weyl fermions are *massless* quasiparticles that exist in Weyl semimetals (WSMs) such as TaAs, NbP, and MoTe$_2$, which have a band structure exhibiting zero energy gap points called Weyl nodes [8]. The Weyl nodes come in pairs with opposite chirality (positive and negative), which are separated slightly in momentum space. The *chirality* (or handedness) of Weyl fermions means that their spin is locked either along (right-handed) or against (left-handed) the direction of motion, which, for massless particles, is the same as the property of *helicity*. The spin-locking reduces scattering and provides a more stable transport of charge than conventional electron flow. In addition, the reduced

sensitivity of Weyl fermion wavefunctions to interactions with the environment could also lead to more stable devices and circuits that exploit these properties. The WSMs are three-dimensional (3-D) analogs of the two-dimensional graphene material. The carrier velocity in WSMs is theoretically *twice* as fast as in graphene, but Weyl transport occurs in 3-D, for greater flexibility in device design than with the 2-D transport in graphene. The exotic behavior of Weyl fermions suggests unusual and novel applications. For instance, the exceptionally high electron mobilities could lead to faster, lower energy circuits, ushering in a new era of "Weyltronics". Electrical currents in Weyl semimetals may be nearly *dissipationless*, but these properties are not yet well understood. Currently the high power dissipation of integrated circuits is a fundamental roadblock to greater performance and integration density. A Weyl device concept is shown in the right-hand panel of Fig. 14 [9]. Weyl fermions are investigated at the University of Delaware for low SWAP-C devices and circuits.

4.4. **Weyl Fermion Device Characterization**. To explore the characteristics and limitations of Weyl semimetals for low power electronics, prototype device structures were fabricated and measured. We began by using GeSn alloys with high Sn contents so that the bandgap energy would be near zero [4,6]. It is possible, but not yet verified, that zero bandgap GeSn may be a Weyl semimetal, or at least have the massless Dirac points that allow very high carrier velocities for low power circuits. Device fabrication started with a semi-insulating GaAs substrate, and the GeSn layers were grown by MBE. Standard photolithography was used to pattern the negative photoresist (NR9-3000PY) into electrical contacts, with dimensions and geometry as shown in Fig. 14. The top contact electrode was made from layers of evaporated Ti/Pt/Ag. Dice containing several devices were cut using a diamond edged saw, producing the structures shown in the middle panel of Fig. 14. Electrical characteristics were measured across different pairs of contacts with a current-voltage (I-V) parameter analyzer, as shown in Fig. 15 (left panel). As expected, the resistance across several regions (R_{15}) was higher than across a single region (R_{23}). A metal electrode was evaporated on the back of the wafer to form a transistor structure similar to that in Fig. 14 (right panel) and to study the possibility of gate control of the current, which was successfully shown in Fig. 15 (right panel). These experimental results suggested that GeSn devices may be worthy of further study for Army applications requiring high speed, low-power operation.
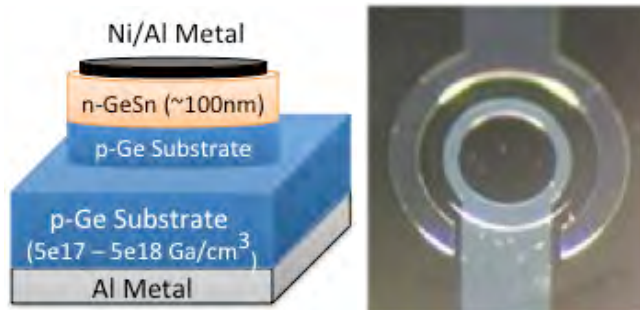
Figure 12. Left panel shows the layer diagram of a GeSn/Ge n-p heterojunction diode. Right panel shows top-view micrograph of a fabricated GeSn diode, where the shiny annular rings are the metal contacts to the darker gray GeSn semiconductor regions.
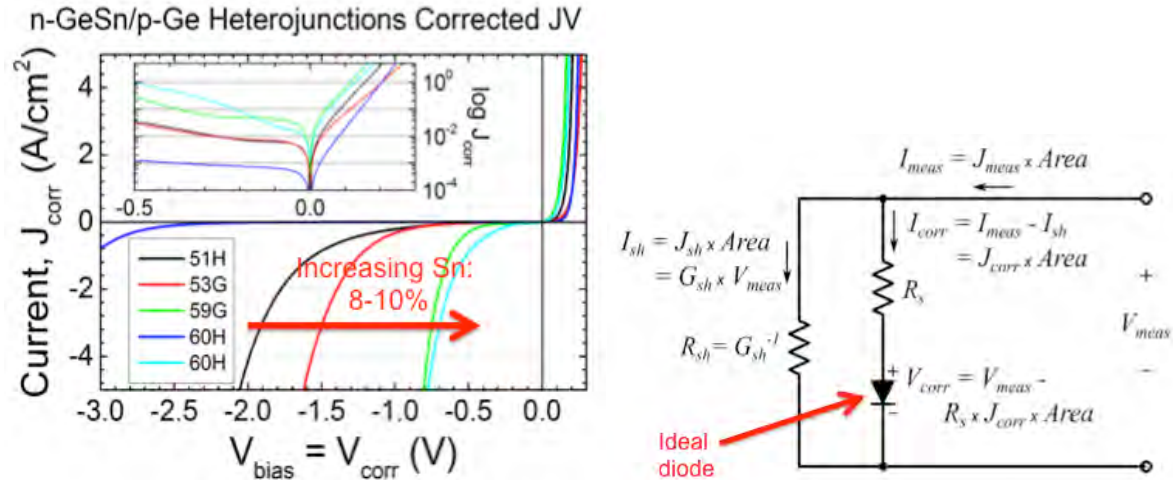
Figure 13. (a. Left Panel) The measured I-V characteristics of GeSn/Ge n-p heterojunction diodes, with different Sn contents, in which the leakage current and series resistance were analytically removed. With increasing Sn content, the magnitude of the reverse breakdown voltage decreased. **(b. Right Panel)** Equivalent circuit model that was used to analytically remove the effects of shunt leakage conductance (G_{sh}) and bulk series resistance (R_s).
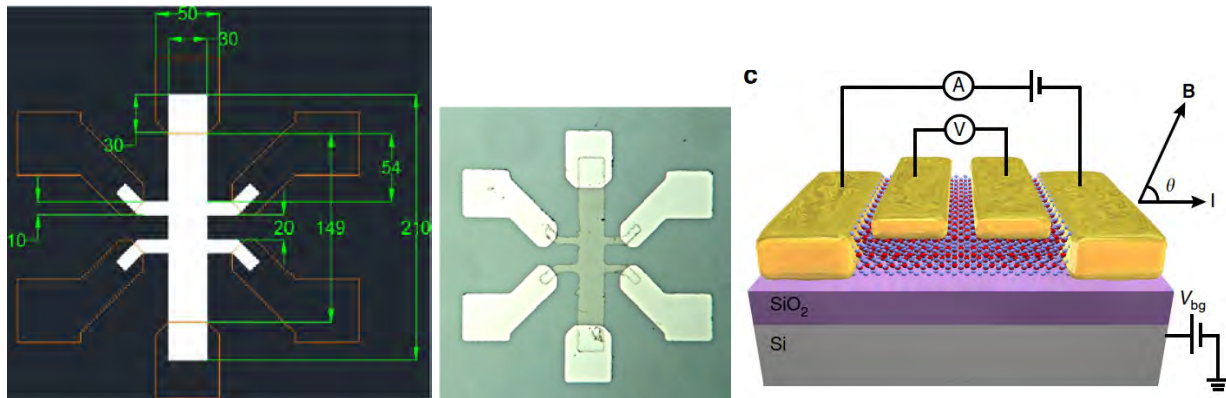
Figure 14. Left panel shows the design and dimensions of the 6-terminal Hall bar geometry used for transport measurements of Weyl semimetals. Middle panel shows top-view micrograph of a fabricated Hall device, from a sample of GeSn with 20% Sn on a semi-insulating GaAs substrate (SGS215), with deposited metal electrode layers of Ti (5 nm), Pt (10 nm), Ag (300 nm). Right panel shows a Weyl device concept, with the Weyl SM (shown as a ball/stick region) deposited on top of an SiO_2 layer, and with gold electrodes on top [9].

15
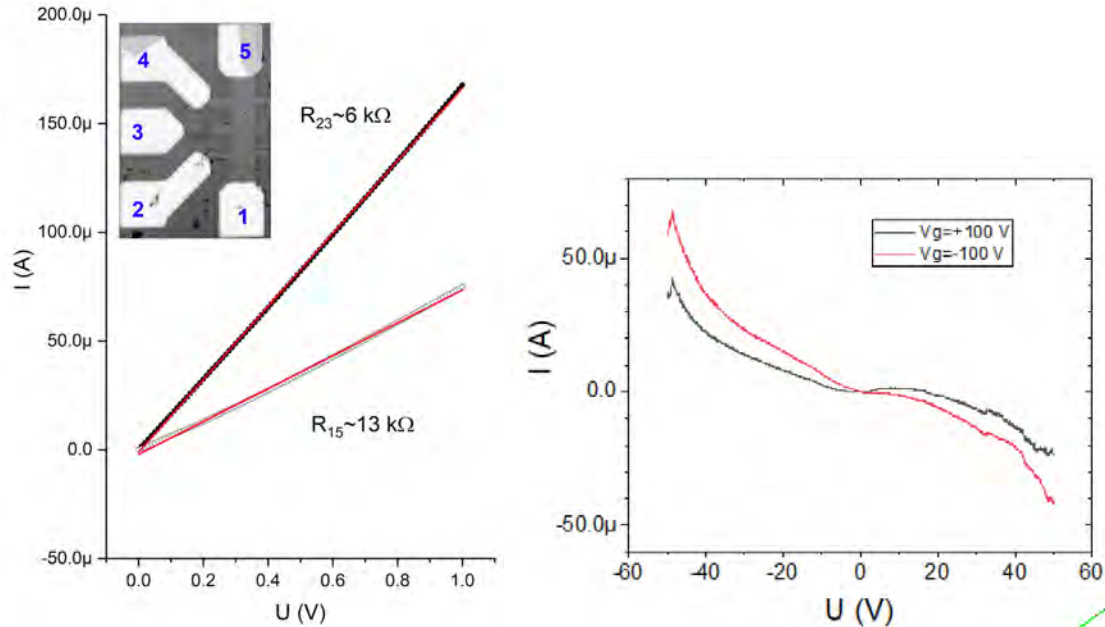
Figure 15. Left panel shows the measured current versus voltage (I-V) characteristics between neighboring contacts on the GeSn Hall bar (sample SGS215_1_S13), giving the resistance. A semiconductor Parameter Analyzer HP 4156B with standard probes was used for the measurements. Right panel shows that an applied back gate voltage affects the current of a transistor-like structure. The reason for the relatively high voltages was that the back gate electrode was placed on the bottom of the insulating substrate, which was about 610 μm thick, rather than on a much thinner top surface insulator. A thinner gate electrode should significantly lower the operating voltages.

(6) Bibliography (Publications and References)

1. J. Hart, T. Adam, Y. Kim, Y.-C. Huang, A. Reznicek, R. Hazbun, J. Gupta, and J. Kolodzey, "Temperature varying photoconductivity of GeSn alloys Grown by CVD with Sn concentrations from 4% to 11%," J. Appl. Phys., v. 119, 093105, 2016; doi:10.1063/1.4942851.

2. R. Hickey, N. Fernando, J. Hart, R. Hazbun, S. Zollner, and J. Kolodzey, "Properties of pseudomorphic and relaxed Germanium Tin alloys (x < 0.185) grown by MBE," J. Vacuum Science & Technology B: Nano, v. 35 (2), 021205, 2017; doi: http://dx.doi.org/10.1116/1.4975149.

3. N.S. Fernando, R.A. Carrasco, R. Hickey, J. Hart, R. Hazbun, S. Schoeche, J.N. Hilfiker, J. Kolodzey, and S. Zollner, "Band gap and strain engineering of pseudomorphic $Ge_{1-x-y}Si_xSn_y$ alloys on Ge and GaAs for photonic applications," J. Vacuum Science & Technology B, Nanotechnology and Microelectronics: Materials, Processing, Measurement, and Phenomena 36, 021202 (2018); https://doi.org/10.1116/1.5001948.

16

4. Dominic Imbrenda, Ryan Hickey, Rigo Carrasco, Nalin S. Fernando, Jeremy VanDerslice, Stefan Zollner, and James Kolodzey, "Infrared dielectric response, index of refraction, and absorption of germanium-tin alloys with tin contents up to 27% deposited by molecular beam epitaxy," Appl. Phys. Lett., 2018, submitted.

5. A.V. Andrianov, J.P. Gupta, J. Kolodzey, V.I. Sankin, A.O. Zakhar'in, and Yu.B. Vasilyev, "Current injection induced terahertz emission from 4H-SiC p-n junctions," Appl. Phys. Lett., v. 103 (22), 221101, 2013; doi: 10.1063/1.4832824.

6. Ryan Hickey, Dominic Imbrenda, James Kolodzey, "Low temperature molecular beam epitaxy growth of germanium tin alloys with up to 31% tin," 2018, manuscript in preparation.

7. https://spectrum.ieee.org/tech-talk/semiconductors/materials/exotic-particles-could-lead-to-faster-electronics

8. https://phys.org/news/2015-12-weyl-fermion-discovery-ten-breakthrough.html

9. Y. Wang, E. Liu, F. Miao, "Gate-tunable negative longitudinal magnetoresistance," Nature Communications, vol. 7, 13142 (2016).

(7) Appendices:

Appendix I. Guide for Installing and Operating Visual Studio with Open CV Software for Image Analysis and Navigation

1. Install Visual Studio

Once you have downloaded Visual Studio (VS), you will need to install it on your computer, as well as installing the types of packages you will need such as the Visual C++ template. One thing that might be problematic is the copy of VS available to students is a 32 bit option and this can cause issues when trying to work with Open CV on a 64 bit machine. To get around this you can try using a 32 bit virtual machine and see if that helps.

2. Install Open CV & Configure with VS

In order to best track paths in VS, you will need to install Open CV. This can be done by downloading Open CV from their website: http://opencv.org/ and following an install guide video like the one provided here: https://www.youtube.com/watch?v=l4372qtZ4dc .

3. Sample project

Once everything is installed, you can explore many sample projects on Github for C++ Open CV tracking. Below is the source code for one such project that I found useful and slightly modified for the project.

```cpp
#include "opencv2/video/tracking.hpp"
#include "opencv2/imgproc/imgproc.hpp"
#include "opencv2/videoio/videoio.hpp"
#include "opencv2/highgui/highgui.hpp"

#include <iostream>
#include <ctype.h>

    using namespace cv;
using namespace std;

static void help()
{
    // print a welcome message, and the OpenCV version
    cout << "\nThis is a demo of Lukas-Kanade optical flow lkdemo(),\n"
            "Using OpenCV version " << CV_VERSION << endl;
    cout << "\nIt uses camera by default, but you can provide a path to video as an
argument.\n";
    cout << "\nHot keys: \n"
            "\tESC - quit the program\n"
            "\tr - auto-initialize tracking\n"
            "\tc - delete all the points\n"
            "\tn - switch the \"night\" mode on/off\n"
            "To add/remove a feature point click it\n" << endl;
}

Point2f point;
bool addRemovePt = false;
```

```cpp
static void onMouse(int event, int x, int y, int /*flags*/, void* /*param*/)
{
        if (event == EVENT_LBUTTONDOWN)
        {
                point = Point2f((float)x, (float)y);
                addRemovePt = true;
        }
}

int main(int argc, char** argv)
{
        //String filename = "Aptina1.mp4";
        //VideoCapture capture(filename);
        VideoCapture capture;

        TermCriteria termcrit(TermCriteria::COUNT | TermCriteria::EPS, 20, 0.03);
        Size subPixWinSize(10, 10), winSize(31, 31);

        const int MAX_COUNT = 1000;
        bool needToInit = true;
        bool nightMode = false;

        cv::CommandLineParser parser(argc, argv, "{@input||}{help h||}");
        string input = parser.get<string>("@input");
        if (parser.has("help"))
        {
                help();
                return 0;
        }
        if (input.empty())
                capture.open(0);
        else if (input.size() == 1 && isdigit(input[0]))
                capture.open(input[0] - '0');
        else
                capture.open(input);

        if (!capture.isOpened())
        {
                cout << "Could not initialize capturing...\n";
                return 0;
        }

        namedWindow("LK Demo", 1);
        setMouseCallback("LK Demo", onMouse, 0);

        Mat gray, prevGray, image, frame;
        vector<Point2f> points[2];

        for (;;)
        {
                /*for (int count; count <= 500; count += 1) {
                        if (count = 500) {
                                needToInit = false;
                        }
                }*/

                capture >> frame;
```

19

```cpp
            if (frame.empty())
                    break;

            frame.copyTo(image);
            cvtColor(image, gray, COLOR_BGR2GRAY);

            if (nightMode)
                    image = Scalar::all(0);

            if (needToInit)
            {
                    // automatic initialization
                    goodFeaturesToTrack(gray, points[1], MAX_COUNT, 0.01, 10, Mat(), 3,
0, 0.04);
                    cornerSubPix(gray, points[1], subPixWinSize, Size(-1, -1),
termcrit);
                    addRemovePt = false;
            }
            else if (!points[0].empty())
            {
                    vector<uchar> status;
                    vector<float> err;
                    if (prevGray.empty())
                            gray.copyTo(prevGray);
                    calcOpticalFlowPyrLK(prevGray, gray, points[0], points[1], status,
err, winSize,
                            3, termcrit, 0, 0.001);
                    size_t i, k;
                    for (i = k = 0; i < points[1].size(); i++)
                    {
                            if (addRemovePt)
                            {
                                    if (norm(point - points[1][i]) <= 5)
                                    {
                                            addRemovePt = false;
                                            continue;
                                    }
                            }

                            if (!status[i])
                                    continue;

                            points[1][k++] = points[1][i];
                            circle(image, points[1][i], 3, Scalar(0, 255, 0), -1, 8);
                    }
                    points[1].resize(k);
            }

            if (addRemovePt && points[1].size() < (size_t)MAX_COUNT)
            {
                    vector<Point2f> tmp;
                    tmp.push_back(point);
                    cornerSubPix(gray, tmp, winSize, Size(-1, -1), termcrit);
                    points[1].push_back(tmp[0]);
                    addRemovePt = false;
            }

            needToInit = false;
```

```cpp
            imshow("LK Demo", image);

            char c = (char)waitKey(10);
            if (c == 27)
                    break;
            switch (c)
            {
            case 'r':
                    needToInit = true;
                    break;
            case 'c':
                    points[0].clear();
                    points[1].clear();
                    break;
            case 'n':
                    nightMode = !nightMode;
                    break;
            }

            std::swap(points[1], points[0]);
            cv::swap(prevGray, gray);
    }

    return 0;
}
```

Appendix II. Division Review Information Report for March 2018

Advanced Infrared and Terahertz Devices for Navigation, Imaging, Timing, and Ranging
James Kolodzey, University of Delaware, March 2018

(1) NUMBER of peer-reviewed journal publications, number of peer-reviewed conference publications, number of manuscripts, for 2016-2017 (combined for two years).

Number of peer-reviewed journal publications for 2016-2017: five (5)

Number of peer-reviewed conference publications for 2016-2017: five (5)

Number of manuscripts for 2016-2017: three (3) [journal submissions are in progress]

(2) NUMBER of graduate students, number of postdocs for EACH of 2016, 2017, supported under the project(s)

Number of graduate students for 2016: 1

Number of graduate students for 2017: 1

Number of postdocs for 2016: 0

Number of postdocs for 2017: 0

(3) LIST of awards and honors: Make sure that the year is included.

None.

(4) LIST of transitions of your research (to the Army, DoD, Government, Industry): Make sure to include the science (algorithm, method, software, etc.), customer (name and organization), application, and customer investments (money, equipment, personnel):

(a) Provided samples of germanium-tin alloys for optical measurements to: Stefan Schoeche and James N. Hilfiker; J.A. Woollam Co., Inc., 645 M Street, Suite 102, Lincoln, Nebraska 68508

(b) Discussed the commercial potential of infrared detectors and emitters; received equipment donations including Karl Suss MJB-3 mask aligner and semiconductor wafer substrates With David T. Beatson (General Manager), Kevin Lascola (Product Line Manager),

and Christopher Pinzone (Senior Scientist); Thorlabs Quantum Electronics, 10335 Guilford Rd, Jessup, MD 20794

(c) Measured the infrared photoconductivity of germanium-tin alloys obtained from Yihwan Kim and Yi-Chiau Huang, Applied Materials, Sunnyvale, California 94085, USA

(d) Meetings and technical discussions about computer vision-based navigation and tracking systems for personnel with Gary Katulka, Adam Schofield, and Kevin Johnson, of the US Army CERDEC at Aberdeen Proving Ground (APG). Helped organize the teaching of a course on the fabrication of micro-electro mechanical systems (MEMS) at the University of Delaware by Adam Schofield.

LIST joint publication(s) between PI and government (including DoD) personnel:

None

REPORT OF INVENTIONS AND SUBCONTRACTS
(Pursuant to "Patent Rights" Contract Clause) (See Instructions on back)

The public reporting burden for this collection of information is estimated to average 1 hour per response, including the time for reviewing instructions, searching existing data sources, gathering and maintaining the data needed, and completing and reviewing the collection of information. Send comments regarding this burden estimate or any other aspect of this collection of information, including suggestions for reducing the burden, to the Department of Defense, Executive Services Directorate (9000-0095). Respondents should be aware that notwithstanding any other provision of law, no person shall be subject to any penalty for failing to comply with a collection of information if it does not display a currently valid OMB control number.

PLEASE DO NOT RETURN YOUR COMPLETED FORM TO THE ABOVE ORGANIZATION. RETURN COMPLETED FORM TO THE CONTRACTING OFFICER.

1.a. NAME OF CONTRACTOR/SUBCONTRACTOR	2.a. NAME OF GOVERNMENT PRIME CONTRACTOR	3. TYPE OF REPORT (X one)
University of Delaware	Office of Naval Research	a. INTERIM ☐ b. FINAL ☒

1.b. ADDRESS *(Include ZIP Code)*
210 Hullihen Hall
Newark, DE 19716

2.b. ADDRESS *(Include ZIP Code)*
100 Alabama Strt, NW, Suite 4R15
Atlanta, GA 30303-3104

4. REPORTING PERIOD *(YYYYMMDD)*
a. FROM 20120803
b. TO 20180311

1.c. CONTRACT NUMBER
W911NF-12-1-0380

1.d. AWARD DATE *(YYYYMMDD)*
20120803

2.c. CONTRACT NUMBER
W911NF-12-1-0380

2.d. AWARD DATE *(YYYYMMDD)*
20120803

SECTION I - SUBJECT INVENTIONS

5. "SUBJECT INVENTIONS" REQUIRED TO BE REPORTED BY CONTRACTOR/SUBCONTRACTOR *(If "None," so state)*

NAME(S) OF INVENTOR(S) (Last, First, Middle Initial) a.	TITLE OF INVENTION(S) b.	DISCLOSURE NUMBER, PATENT APPLICATION SERIAL NUMBER OR PATENT NUMBER c.	ELECTION TO FILE PATENT APPLICATIONS (X) (1) UNITED STATES (a) YES / (b) NO	ELECTION TO FILE PATENT APPLICATIONS (X) (2) FOREIGN (a) YES / (b) NO	CONFIRMATORY INSTRUMENT OR ASSIGNMENT FORWARDED TO CONTRACTING OFFICER (X) e. (a) YES / (b) NO
NONE					

f. EMPLOYER OF INVENTOR(S) NOT EMPLOYED BY CONTRACTOR/SUBCONTRACTOR

(1) (a) NAME OF INVENTOR (Last, First, Middle Initial)	(2) (a) NAME OF INVENTOR (Last, First, Middle Initial)
(b) NAME OF EMPLOYER	(b) NAME OF EMPLOYER
(c) ADDRESS OF EMPLOYER (Include ZIP Code)	(c) ADDRESS OF EMPLOYER (Include ZIP Code)

g. ELECTED FOREIGN COUNTRIES IN WHICH A PATENT APPLICATION WILL BE FILED

(1) TITLE OF INVENTION	(2) FOREIGN COUNTRIES OF PATENT APPLICATION

SECTION II - SUBCONTRACTS (Containing a "Patent Rights" clause)

6. SUBCONTRACTS AWARDED BY CONTRACTOR/SUBCONTRACTOR *(If "None," so state)*

NAME OF SUBCONTRACTOR(S) a.	ADDRESS (Include ZIP Code) b.	SUBCONTRACT NUMBER(S) c.	FAR "PATENT RIGHTS" (1) CLAUSE NUMBER	FAR "PATENT RIGHTS" d. (2) DATE (YYYYMM)	DESCRIPTION OF WORK TO BE PERFORMED UNDER SUBCONTRACT(S) e.	SUBCONTRACT DATES (YYYYMMDD) f. (1) AWARD	SUBCONTRACT DATES (YYYYMMDD) f. (2) ESTIMATED COMPLETION
NONE							

SECTION III - CERTIFICATION

7. CERTIFICATION OF REPORT BY CONTRACTOR/SUBCONTRACTOR *(Not required if: (X as appropriate))* SMALL BUSINESS or ☐ NONPROFIT ORGANIZATION ☐

I certify that the reporting party has procedures for prompt identification and timely disclosure of "Subject Inventions," that such procedures have been followed and that all "Subject Inventions" have been reported.

a. NAME OF AUTHORIZED CONTRACTOR/SUBCONTRACTOR OFFICIAL (Last, First, Middle Initial)	b. TITLE	c. SIGNATURE	d. DATE SIGNED
Jill M. Vamos	Sponsored Research Accountant	*(signed)*	6132018

DD FORM 882, JUL 2005   PREVIOUS EDITION IS OBSOLETE.   FormFlow/Adobe Professional 6.0